J Appl Electrochem (2011) 41:299–305
DOI 10.1007/s10800-010-0238-z

ORIGINAL PAPER

Effects of various factors on capacitive properties of $VO_x \cdot nH_2O$ powders in aqueous electrolyte

Lian Mei Chen · Qiong Yu Lai · Hong Mei Zeng · Yan Jing Hao · Jian Hua Huang

Received: 6 February 2010 / Accepted: 24 October 2010 / Published online: 10 November 2010

Abstract In this work, effects of drying temperature, pH of aqueous electrolyte and current density on capacitive performance of $VO_x \cdot nH_2O$ material were firstly investigated. $VO_x \cdot nH_2O$ powders were prepared by a melt quenching method. The samples were characterized by X-ray diffraction analysis (XRD) and Fourier transform infrared (FTIR). The capacitive properties of $VO_x \cdot nH_2O$ samples were examined by cyclic voltammetry and galvanostatic charge/discharge test. $VO_x \cdot nH_2O$ sample which was obtained at the drying temperature of 80 °C, delivers a maximum specific capacitance of 227.3 F g^{-1} and exhibits excellent capacity retention in the potential range of −0.3 to 0.7 V at a current density of 200 mA g^{-1} in $NaNO_3$ solution with pH 2.

Keywords $VO_x \cdot nH_2O$ · Capacitive properties · Drying temperature · pH

1 Introduction

Supercapacitors are very interesting charge-storage devices with high energy density and high power density. Recently, they have attracted worldwide attention due to their potential applications in hybrid electric vehicles, back-up power storage, peak power sources, and so on [1, 2]. Based on the charge-storage mechanism, supercapacitors are classified as: electric double-layer capacitors (EDLCs) that store charge by utilizing the double-layer capacitance at an electrode/electrolyte interface; and pseudo-capacitors that store charge by utilizing the pseudo-capacitance arising from fast and reversible Faradaic reactions of electroactive materials with several oxidation states [3, 4]. Compared with EDLCs, more research has been focused on pseudo-capacitors which have higher specific capacitance. Traditionally, hydrous ruthenium oxide ($RuO_2 \cdot xH_2O$) has been an ideal electrode material for pseudo-capacitors since it exhibits excellent pseudo-capacitive behavior with great specific capacitance and good reversibility in strong acidic electrolyte [5–8]. Unfortunately, its large-scale application is unfeasible owing to its high cost and rarity in natural resource. Therefore, more economical transition-metal oxides (such as MnO_2, NiO, and V_2O_5, etc.) are considered as promising alternative electrode materials for supercapacitors [9–14].

Among these transition-metal oxides, V_2O_5 is an attractive electrode material because of its low-cost, modest electronic conductivity, easy preparation, as well as several stable oxidation states. The application of V_2O_5 in Lithium-ion rechargeable battery has been widely recognized and well studied [15–17], but there are few reports about V_2O_5 as electrode material for pseudo-capacitor. Lee et al. [18] firstly reported that amorphous V_2O_5 displayed 350 F g^{-1} between −0.2 and 0.8 V in an aqueous KCl electrolyte with pH 6.67. After 100 cycles, the specific capacitance rapidly declined to about 200 F g^{-1}. Later, Reddy et al. [19] prepared nano-porous V_2O_5 with crystalline structure, which delivered an initial specific capacitance of 214 F g^{-1} and exhibited poor cycling life in 2 mol L^{-1} KCl solution. Jayalakshmi et al. [20] applied a

L. M. Chen · Q. Y. Lai (✉) · H. M. Zeng · Y. J. Hao · J. H. Huang
College of Chemistry, Sichuan University, Chengdu 610064, People's Republic of China
e-mail: Laiqy5@hotmail.com

L. M. Chen
Chemical Synthesis and Pollution Control Key Laboratory of Sichuan Province, China West Normal University, Nanchong, Sichuan 637000, People's Republic of China

thermal decomposition method to synthesize crystal V_2O_5 powders that showed a fairly low specific capacitance of 12 F g^{-1} in 0.1 mol L^{-1} KCl solution. Therefore, further research is still needed to improve capacitive performance of vanadium oxide. In this article, $VO_x{\cdot}nH_2O$ samples were prepared by a melt quenching method. The effects of drying temperature, pH of aqueous electrolyte, and current density on capacitive behavior of $VO_x{\cdot}nH_2O$ were firstly discussed, and then the optimum conditions were obtained.

2 Experimental

2.1 Preparation of $VO_x{\cdot}nH_2O$ powders

$VO_x{\cdot}nH_2O$ powders were prepared by a melt quenching method. Crystalline V_2O_5 powders were melted at 800 °C in a muffle furnace. After being heated for 20 min, the melt was quickly quenched into distilled water with stirring. After 2 h, the formed brownish sol was filtered to remove a small quantity of insoluble impurities. The sol was constantly stirred until gels were formed. Finally, the gels were dried at 40, 80, 120, 160, 200, 240 °C under vacuum, respectively. The obtained $VO_x{\cdot}nH_2O$ samples were correspondingly labeled as VO-1#, VO-2#, VO-3#, VO-4#, VO-5#, and VO-6#.

2.2 Characterization of $VO_x{\cdot}nH_2O$ samples

The samples were characterized by X-ray diffraction (XRD) using a D/max-rA diffractometer with Cu K_α radiation operated at 40 kV and 100 mA in the range of 10–70° ($\lambda = 0.15418$ nm). Fourier transform infrared (FTIR) spectra were obtained by Perkin-Elmer 16 pc. The samples were mixed with KBr and examined in the wave number range of 400–4000 cm^{-1}.

2.3 Electrochemical measurements

The $VO_x{\cdot}nH_2O$ electrode was prepared by mixing $VO_x{\cdot}nH_2O$ powders with acetylene black and polyvinyidene fluoride (PVDF) binder (in a weight ratio of 70:25:5) and grinding the mixture with *N*-methy1-2-pyrrolidine (NMP) as the solvent. The formed slurry was dried in air with infrared lamp to evaporate the NMP solvent. The resulting mixture powders were pressed onto stainless steel mesh (diameter is 5 mm), and then dried at 60 °C under vacuum to remove the residual solvent. The typical mass of active material on a $VO_x{\cdot}nH_2O$ electrode was approximately 1.5 mg.

The cyclic voltammetry (CV) was conducted in a three-electrode system comprising a $VO_x{\cdot}nH_2O$ electrode, a platinum electrode and a saturated calomel electrode (SCE) that serve as the working, counter, and reference electrode, respectively. The tests were carried out with LK2005 electrochemical workstation system in 1 mol L^{-1} $NaNO_3$ solutions with various pH values.

The charge/discharge test was performed in a two-electrode cell fabricated with two $VO_x{\cdot}nH_2O$ electrodes which were separated by a Teflon gasket (inner-diameter of 5 mm, thickness of 3 mm). The experiments were carried out by Neware battery program-control testing system in 1 mol L^{-1} $NaNO_3$ solutions with pH 7 and pH 2.

3 Results and discussion

3.1 IR and XRD analysis

The IR spectra of VO-2#, VO-4#, VO-5#, and pure crystalline V_2O_5 powders as starting material are shown in Fig. 1. The weak absorbance peak at 1627 cm^{-1} is assigned to the bending vibration of O–H, confirming residual water within these samples. In Fig. 1a, the strong peaks at 1006, 757, and 528 cm^{-1} are the IR signature of V_2O_5 xerogel, which are assigned to the stretching vibration peak of V=O, the asymmetric and symmetric stretching vibration peaks of V–O–V, respectively [21]. Similarly, the three strong peaks corresponding to V_2O_5 xerogel are also observed in Fig. 1b and c. These data indicate that the main ingredient in $VO_x{\cdot}nH_2O$ samples is V_2O_5, in which vanadium oxidation state is V(V).

Compared to pure crystalline V_2O_5 (Fig. 1d), the V=O absorbance peaks of VO-2#, VO-4#, and VO-5# shift to lower frequency, which should be resulted from the existence of V(IV) in $VO_x{\cdot}nH_2O$ [22, 23]. The formation of V(IV) could be attributed to two factors: (i) the decomposition of the melting V_2O_5 [24, 25]; (ii) the interaction of water with V_2O_5 xerogel [26]. As we know, V_2O_5 is *n*-type

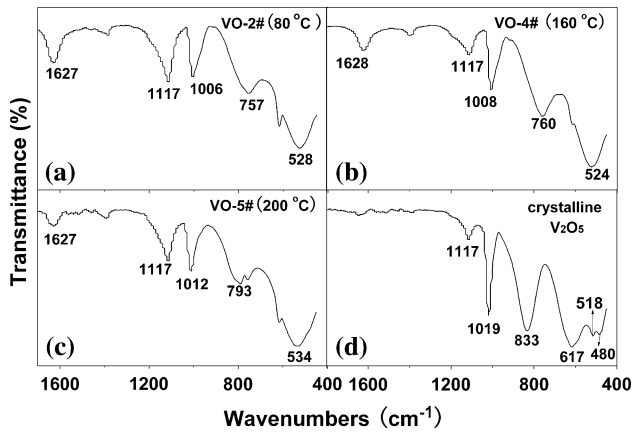

Fig. 1 IR spectra of $VO_x{\cdot}nH_2O$ samples prepared at different drying temperatures

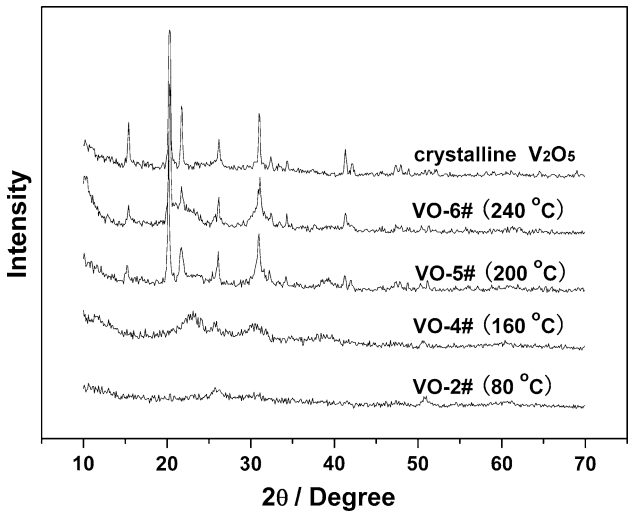

Fig. 2 XRD patterns of $VO_x{\cdot}nH_2O$ samples prepared at different drying temperatures

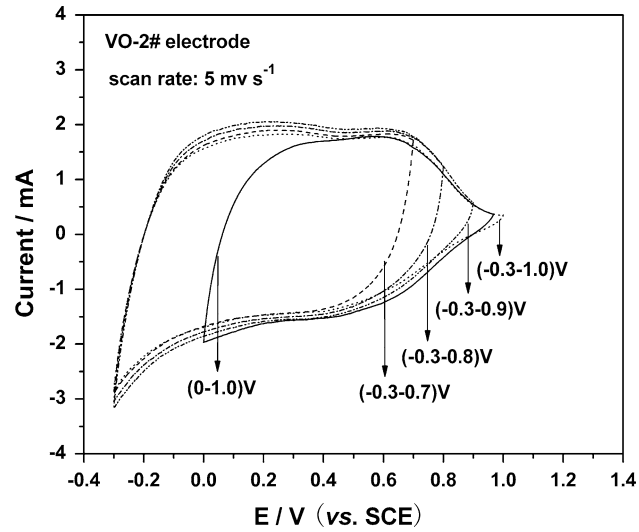

Fig. 3 CV curves of VO-2# electrode in various potential ranges in neutral $NaNO_3$ solution

semiconductor, and its charge transport proceeds via electron hopping along $V^{4+} \rightarrow O \rightarrow V^{5+}$, so the $VO_x{\cdot}nH_2O$ samples would have higher electronic conductivity than pure crystalline V_2O_5 because of the existence of V(IV) [27, 28].

One can also observe in Fig. 1 that the V=O peak of $VO_x{\cdot}nH_2O$ sample shifts to higher frequency with increasing temperature, which should be caused by the decrease of V(IV) concentration. Liu et al. [23] have found that the oxidation of V(IV) to V(V) occurs at high temperature, resulting in the V=O bond length shortening and its absorbance peak blueshift. Of course, the declining content of V(IV) would lead to lower electronic conductivity and worse capacitive performance.

Figure 2 displays XRD patterns of the $VO_x{\cdot}nH_2O$ samples prepared at different drying temperatures. No distinct diffraction peaks are noted for the samples prepared below 160 °C. Instead, some peaks appear for the samples prepared above 160 °C. The XRD results suggest that $VO_x{\cdot}nH_2O$ samples are amorphous when dried below 160 °C, and become crystalline at higher temperature.

3.2 Electrochemical analysis

3.2.1 Cyclic voltammetry test

In order to find out the optimal potential range of $VO_x{\cdot}nH_2O$ material, VO-2# electrode was examined with cyclic voltammetry (CV) in various potential ranges. Figure 3 presents the measured CV curves of VO-2# electrode in neutral $NaNO_3$ solution at a scan rate of 5 mV s^{-1}. Obviously, the output current evidently declines when the charge voltage is above 0.7 V (vs. SCE). The VO-2# electrode still exhibits good capacitive performance when discharge voltage is declined to −0.3 V (vs. SCE). Hence, the suitable working potential window is between −0.3 and 0.7 V for $VO_x{\cdot}nH_2O$ material.

The pH value of aqueous electrolyte is another crucial factor in determining the capacitive behavior of $VO_x{\cdot}nH_2O$ powders. VO-2# electrode was also examined with cyclic voltammetry in alkaline and acid $NaNO_3$ solution. The pH value of $NaNO_3$ solution was adjusted with HNO_3 or NaOH solution.

The CV curves of VO-2# electrode in alkaline $NaNO_3$ solutions with various pH values are shown in Fig. 4. The output current rapidly decreases with the pH value increasing from 7 to 13, revealing that the capacitive properties of $VO_x{\cdot}nH_2O$ become worse. V_2O_5, as the main ingredient of $VO_x{\cdot}nH_2O$ sample, is amphoteric oxide, so $VO_x{\cdot}nH_2O$ can be easily dissolved in alkaline solution (shown in reaction 1), which would result in poor capacitive performance:

$$V_2O_5 + 6OH^- \rightarrow 2VO_4^{3-} + 3H_2O. \quad (1)$$

Figures 5 and 6 give CV curves of VO-2# electrode in acid $NaNO_3$ solutions with various pH values. It can be found in Fig. 5 that the output current slightly increases with the pH value dropping from 7 to 3, and evidently increases at pH 2. However, the current remarkably decreases with increasing cycle number at pH 1 (Fig. 6), indicating that an irreversible reaction occurs. The acidity of V_2O_5 is slightly stronger than its alkalinity, so $VO_x{\cdot}nH_2O$ can be dissolved in the strong acid solution with pH 1 (shown in reaction 2).

$$V_2O_5 + 6H^+ \rightarrow 2VO^{3+} + 3H_2O \quad (2)$$

According to the above results and discussion, the pH value of the aqueous electrolyte for $VO_x{\cdot}nH_2O$ material should be controlled between 7 and 2.

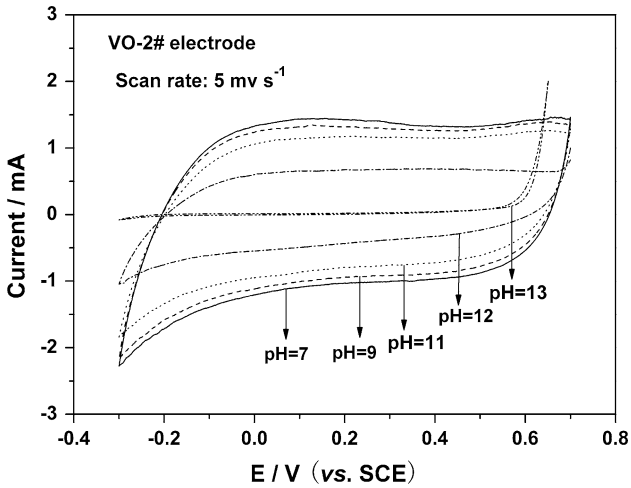

Fig. 4 CV curves of VO-2# electrode in alkaline $NaNO_3$ solutions with various pH values

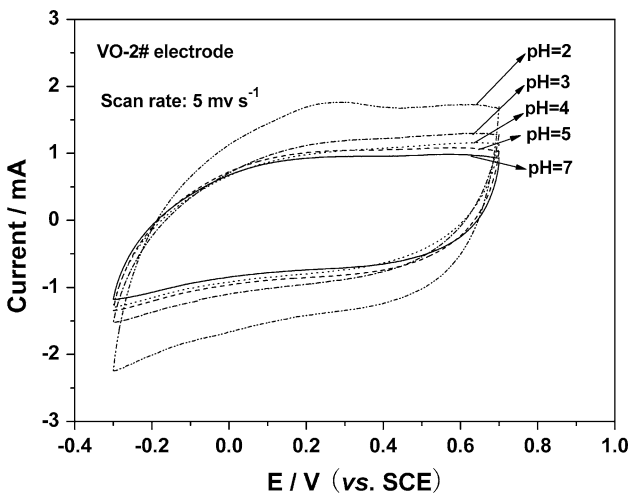

Fig. 5 CV curves of VO-2# electrode in acid $NaNO_3$ solutions with various pH values

3.2.2 Charge and discharge test

The charge/discharge curves of VO-1# to VO-6# in neutral $NaNO_3$ solution at a current density of 200 mA g^{-1} are presented in Fig. 7. All charge/discharge curves are almost linear and the coulombic efficiency is 99–100%, implying that $VO_x{\cdot}nH_2O$ material has an ideal capacitive behavior. Based on the discharge curves, the specific capacitance (C) can be calculated as:

$$C=\frac{2\times I\times \Delta t}{m\times \Delta V} \tag{3}$$

where I, Δt, m, and ΔV, are the current density, discharge time, the active mass of the single electrode and potential window, respectively.

The initial specific capacitance of VO-1# to VO-6# is listed in Table 1. VO-1# delivers a maximum specific capacitance of 229.2 F g^{-1}, while VO-6# delivers the minimum specific capacitance of 115.6 F g^{-1}. Obviously, the special capacitance declines with increasing temperature.

Figure 8 gives cycling life of VO-1# to VO-6# in neutral $NaNO_3$ solution at a current rate of 200 mA g^{-1}. VO-1# and VO-6# have poor cycling performance, but the other samples exhibit relatively good cycling life. Therefore, the most appropriate drying temperature is 80 °C in consideration of specific capacitance and cycling performance.

It can be concluded from Figs. 7 and 8 that $VO_x{\cdot}nH_2O$ samples obtained at different drying temperatures exhibit different specific capacitance values and cycling performance, which should be associated with the structure and water content of $VO_x{\cdot}nH_2O$ samples. XRD analysis reveals that VO-1# to VO-4# is amorphous, but VO-5# and VO-6# are crystalline. Zheng et al. [5, 6] found that amorphous $RuO_2{\cdot}nH_2O$ exhibited better capacitive performance than crystalline RuO_2 did. In our study, VO-6# with well-developed crystalline structure also shows the minimum specific capacitance and the poorest cycling performance.

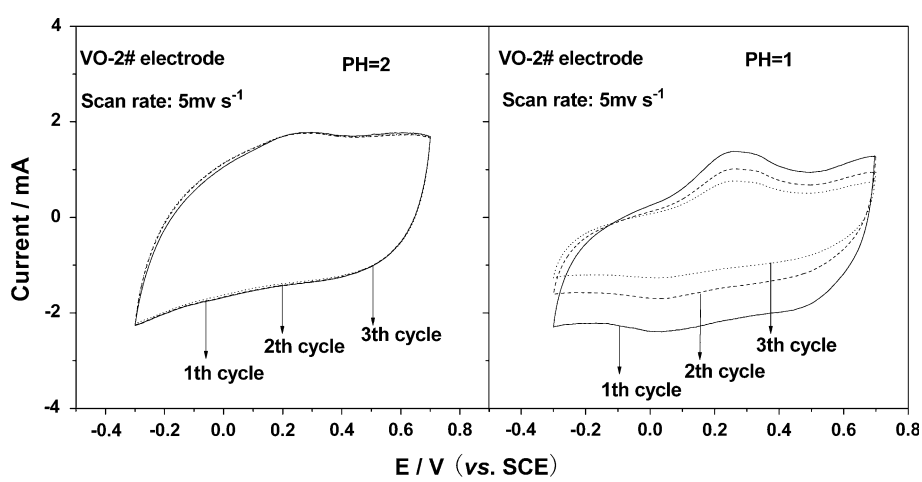

Fig. 6 CV curves of VO-2# electrode in acid $NaNO_3$ solutions with pH 2 and pH 1

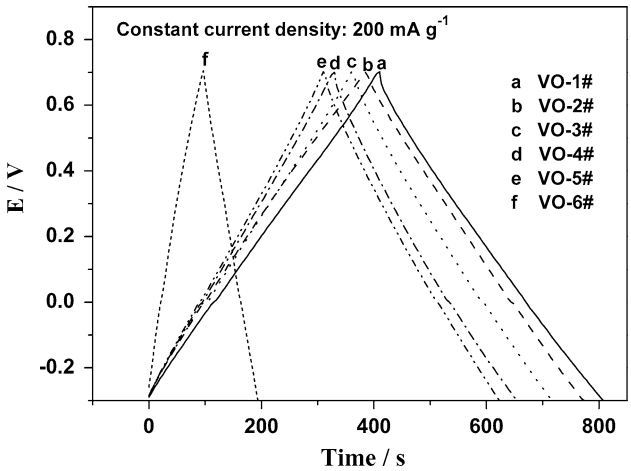

Fig. 7 Charge/discharge curves of $VO_x{\cdot}nH_2O$ samples obtained at different drying temperatures in neutral $NaNO_3$ solution (1#: 40 °C; 2#: 80 °C; 3#: 120 °C; 4#: 160 °C; 5#: 200 °C; and 6#: 240 °C)

Table 1 The water content and specific capacitance of $VO_x{\cdot}nH_2O$ samples prepared at different drying temperatures

$VO_x{\cdot}nH_2O$ sample	Drying temperature (°C)	Water content (wt%)	Discharge specific capacitance (F g^{-1})
VO-1#	40	17.2	229.2
VO-2#	80	13.5	215.9
VO-3#	120	11.9	192.8
VO-4#	160	10.8	177.6
VO-5#	200	8.1	141.2
VO-6#	240	4.7	115.6

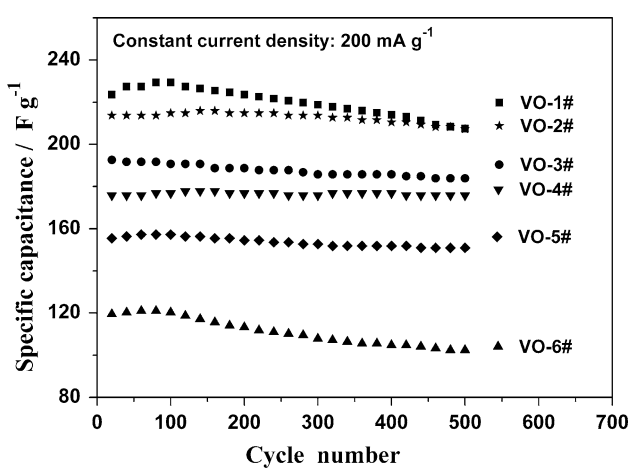

Fig. 8 Cycling life of $VO_x{\cdot}nH_2O$ samples obtained at different drying temperatures in neutral $NaNO_3$ solution (1#: 40 °C; 2#: 80 °C; 3#: 120 °C; 4#: 160 °C; 5#: 200 °C; and 6#: 240 °C)

The VO_x content in the $VO_x{\cdot}nH_2O$ samples was analyzed by oxidation–reduction titration, and then the water content was calculated (Table 1). It can be noted that the water content declines with increasing temperature. The suitable water content not only enhances electronic conductivity (see Sect. 3.1), but also improves ionic adsorption/desorption and protonic diffusion in the bulk [5, 6, 9]. However, excessive water content is unfavorable for cycling life because it would make $VO_x{\cdot}nH_2O$ be easily dissolved in aqueous solution. The water content of VO-1# prepared at 40 °C is up to 17.2 wt%, bringing about its poor cycling performance. The water content of VO-6# prepared at 240 °C is reduced to 4.7 wt%, resulting in the minimum initial specific capacitance. Therefore, the drying temperature of 80 °C is optimum in view of specific capacitance and cycling performance. In the subsequent experiments, VO-2# prepared at 80 °C is selected to investigate other capacitive properties of the $VO_x{\cdot}nH_2O$ material.

Figurs 9 and 10 present the charge/discharge curves and cycling life of VO-2# electrode in $NaNO_3$ solution with pH 2, respectively. The relationship between potential and time is quite linear (Fig. 9). The discharge specific capacitance is firstly 227.3 F g^{-1} and keeps 221.3 F g^{-1} after 600 cycles in $NaNO_3$ solution with pH 2 (Fig. 10). VO-2# electrode delivers higher specific capacitance at pH 2 than that at pH 7, which is related to the energy storage mechanism of $VO_x{\cdot}nH_2O$. It has been found that $MnO_2{\cdot}nH_2O$ has two kinds of energy storage mechanism in aqueous electrolyte, proton–electronic mechanism, and ionic adsorption/desorption mechanism [9–11]. We herewith propose a similar energy storage mechanism for $VO_x{\cdot}nH_2O$ (shown in reactions 4 and 5).

$$VO_a(OH)_b+\delta H^+ +\delta e^- \rightleftharpoons VO_{a-\delta}(OH)_{b+\delta} \quad (4)$$

$$VO_a(OH)_b+\delta Na^+ +\delta e^- \rightleftharpoons Na_\delta VO_a(OH)_b \quad (5)$$

When pH drops from 7 to 2, it becomes easier for reaction 4 to take place because of increasing H^+

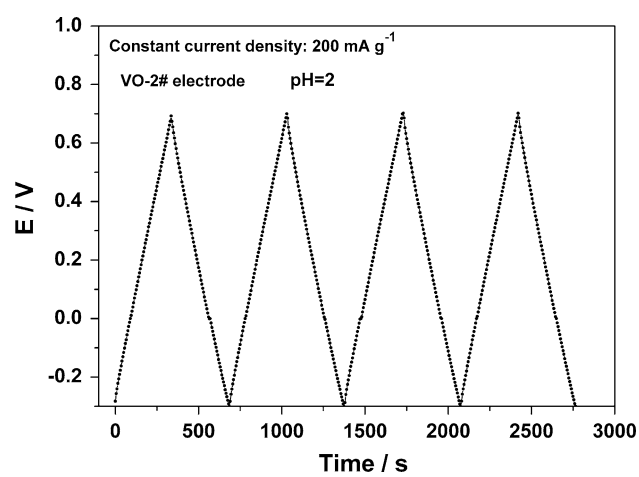

Fig. 9 Charge/discharge curves of VO-2# electrode in $NaNO_3$ solution with pH 2 at a current density of 200 mA g^{-1}

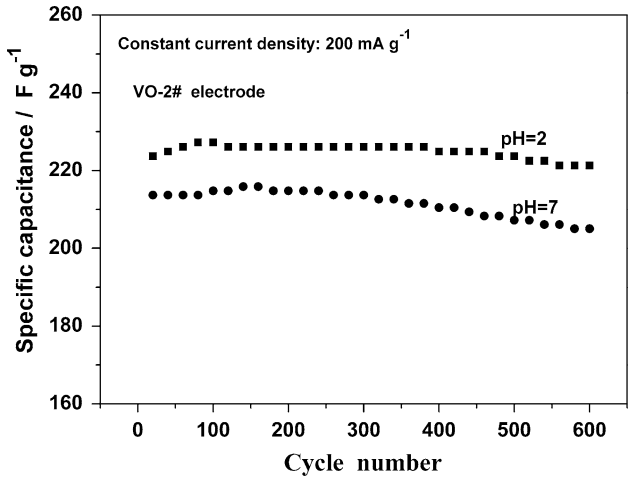

Fig. 10 Cycling life of VO-2# electrode in $NaNO_3$ solutions with pH 2 and pH 7 at a current density of 200 mA g^{-1}

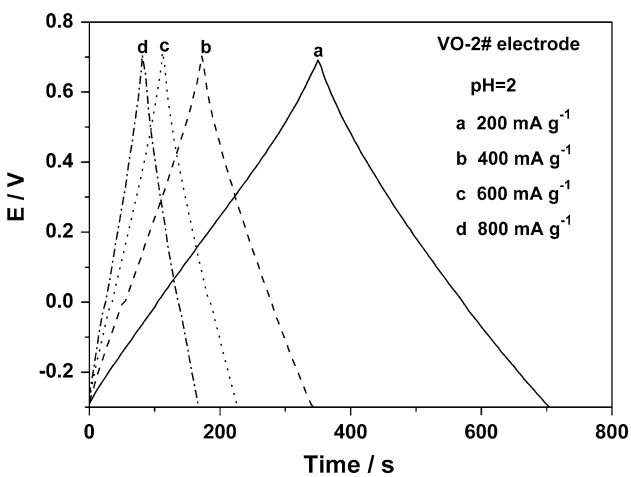

Fig. 11 Charge/discharge curves of VO-2# electrode at different current densities in $NaNO_3$ solution with pH 2

concentration, which would lead to greater specific capacitance.

An ideal electrode material for supercapacitors is able to be charged/discharged at high current density. Figures 11 and 12 show charge/discharge curves and cycling performance of VO-2# electrode at various current densities in $NaNO_3$ solution with pH 2, respectively. A good linear variation of potential versus time is observed in Fig. 11. At the lowest current density of 200 mA g^{-1}, VO-2# electrode delivers the highest specific capacitance of 227.3 F g^{-1}. When current density is increased to 800 mA g^{-1}, the specific capacitance remains 204.5 F g^{-1}. It is obvious that the specific capacitance slightly decreases with increasing current density. In addition, the specific capacitance value is essentially unchanged after 500 cycles at 800 mA g^{-1} (Fig. 12), indicating that VO-2# electrode

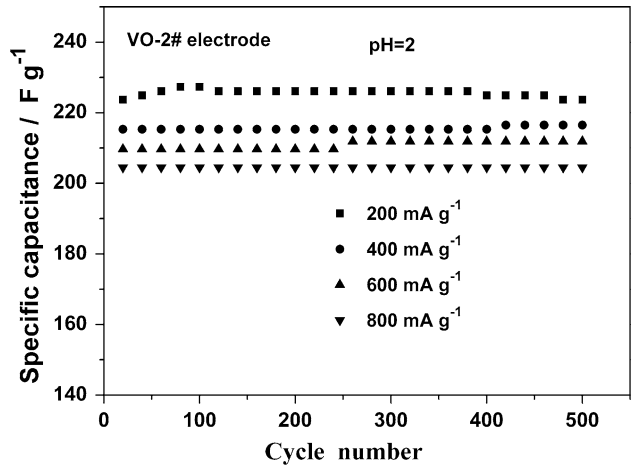

Fig. 12 Cycling performance of VO-2# electrode at different current densities in $NaNO_3$ solution with pH 2

still exhibited good cycling performance at high current density in $NaNO_3$ solution with pH 2.

4 Conclusions

$VO_x{\cdot}nH_2O$ powders were prepared by a melt quenching method. The capacitive properties of $VO_x{\cdot}nH_2O$ samples were strongly affected by drying temperature, pH of aqueous electrolyte, and current density. The optimum drying temperature is 80 °C, and the pH value of aqueous electrolyte should be controlled between 7 and 2. $VO_x{\cdot}nH_2O$ sample which was obtained at 80 °C, delivers a maximum specific capacitance of 227.3 F g^{-1} and exhibits excellent capacity retention in the potential range of −0.3 to 0.7 V at 200 mA g^{-1} in $NaNO_3$ solution with pH 2. The specific capacitance slightly decreases with increasing current density, indicating that $VO_x{\cdot}nH_2O$ powders could be charged/discharged at high current density.

Acknowledgments This work was financially supported by the National Natural Science Foundation of China (No. 20701029) and the Key Program of the China West Normal University (No. 412374).

References

1. Pang SC, Anderson MA, Chapman TW (2000) J Electrochem Soc 147:444
2. Jeong YU, Marthiram A (2001) J Electrochem Soc 148:A189
3. Conway BE (1991) J Electrochem Soc 138:1539
4. Zheng JP, Huang J, Jow TR (1997) J Electrochem Soc 144:2026
5. Zheng JP, Jow TR (1995) J Electrochem Soc 142:L6
6. Zheng JP, Cygan PJ, Jow TR (1995) J Electrochem Soc 142:2699
7. Ramanni M, Haran BS, White RE et al (2001) J Electrochem Soc 148:A374
8. Chang KH, Hu CC (2004) J Electrochem Soc 151:A958
9. Jeong YU, Manthirm A (2002) J Electrochem Soc 149:A1419

10. Wu MQ, Snook GA, Chen GZ et al (2004) Electrochem Commun 6:499
11. Chen Y, Zhang ML, Shi ZH (2005) J Electrochem Soc 152:A1272
12. Donne SW, Hollenkamp AF, Jones BC (2010) J Power Sources 195:367
13. Liu XM, Zhang XG, Fu SY (2006) Mater Res Bull 41:620
14. Patil UM, Salunkhe RR, Gurav KV et al (2008) Appl Surf Sci 255:2603
15. Wang JX, Curtis CJ, Schulz DL et al (2004) J Electrochem Soc 151:A1
16. Adhikary K, Kikkawa S (1997) Solid State Ionics 99:53
17. Mansour AN, Smith PH, Baker WM et al (2002) Electrochim Acta 47:3151
18. Lee HY, Goodenough JB (1999) J Solid State Chem 148:81
19. Reddy RN, Reddy RG (2006) J Power Sources 156:700
20. Jayalakshmi M, Rao MM, Venugopal N et al (2007) J Power Sources 166:578
21. Zhao J, Wang GC, Li XW et al (2007) J Appl Polym Sci 103:2569
22. Chen W, Peng JF, Mai LQ et al (2004) Mater Lett 58:2275
23. Liu XQ, Huang CM, Qiu JW et al (2006) Appl Surf Sci 253:2747
24. Xu WX, Yang SY, Hu XC (1989) Acta Physico Chimica Sinica (Chinese Journal) 5:367
25. Kang A, Livage J, Collongues R (1974) Phys State Solid A 26:175
26. Benmoussa M, Ibnouelghazi E, Bennouna A et al (1995) Thin Solid Films 265:22
27. Muster J, Kim GT, Krstic V et al (2000) Adv Mater 12:420
28. Krins N, Rulmont A, Grandjean J et al (2006) Solid State Ionics 177:3147